Noname manuscript No.
(will be inserted by the editor)

Exploring hyperon structure with electromagnetic transverse densities

Jose Manuel Alarcón · Astrid N. Hiller Blin · Manuel J. Vicente Vacas · Christian Weiss

Received: date / Accepted: date

Abstract We explore the structure of the spin-1/2 flavor-octet baryons (hyperons) through their electromagnetic transverse densities. The transverse densities describe the distribution of charge and magnetization at fixed light-front time and enable a spatial representation of the baryons as relativistic systems. At peripheral distances $b \sim 1/M_\pi$ the transverse densities are computed using a new method that combines chiral effective field theory (χEFT) and dispersion analysis. The peripheral isovector densities arise from two-pion exchange, which includes the ρ resonance through elastic unitarity. The isoscalar densities are estimated from vector meson exchange (ω, ϕ). We find that the "pion cloud" in the charged Σ hyperons is comparable to the nucleon, while in the Ξ it is suppressed. The Λ–Σ^0 transition density is pure isovector and represents a clear manifestiation of peripheral two-pion dynamics.

Keywords Electromagnetic form factors · hyperons · dispersion analysis

1 Introduction

Understanding the structure of strange baryons is an important goal of hadronic physics. The $SU(3)$ octet baryons (hyperons) are stable under strong interac-

J. M. Alarcón
Theory Center, Jefferson Lab, Newport News, VA 23606, USA

A. N. Hiller Blin
Institut für Kernphysik & PRISMA Cluster of Excellence, Johannes Gutenberg Universität, D-55099 Mainz, Germany
E-mail: hillerbl@uni-mainz.de

M. J. Vicente Vacas
Instituto de Física Corpuscular, Universidad de Valencia-CSIC, Institutos de Investigación, Ap. Correos 22085, E-46071 Valencia, Spain

C. Weiss
Theory Center, Jefferson Lab, Newport News, VA 23606, USA

tions and possess an electromagnetic and weak structure similar to that of the nucleon, in terms of vector and axial current matrix elements, which can be measured in radiative transitions and weak decays [1,2]. It is thus possible to characterize the hyperons by charge and current densities and compare these to those in the nucleon. Interesting questions are whether the hyperons are more "compact" or more "extended" than the nucleon, and how they couple to the chiral degrees of freedom responsible for long-range structure ("pion cloud"). The answers to these questions have implications also for the understanding of hyperon-hyperon interactions and the role of strangeness in strong interaction dynamics at low energies; see Ref. [3] for a review.

For relativistic systems such as hadrons the electromagnetic structure can be expressed in terms of transverse densities. They are defined as the 2-dimensional Fourier transforms of the hadron form factors and describe the spatial distribution of charge and current in the system at fixed light-front time $x^+ = x^0 + x^3 = \text{const}$ [4–7]. As such they are boost-invariant and provide an objective representation of the hadron as an extended system. They are closely related to the partonic description of hadron structure in QCD and correspond to a projection of the generalized parton distributions (GPDs). Transverse densities have been used extensively in studies of nucleon structure; see Ref. [8] for a review of results. They can equally well be used to explore hyperon structure and answer the above questions.

At peripheral distances $b \sim 1/M_\pi$ the transverse densities can be computed model-independently using a new method that combines chiral effective field theory (χEFT) and dispersion analysis [9]. The densities are represented as dispersive integrals over the imaginary parts of the baryon form factors on the cut in the timelike region, $\mathrm{Im}\, F^B(t)$ at $t > t_{\rm thr}$. The spectral functions on the two-pion cut ($t_{\rm thr} = 4M_\pi^2$) are constructed using the elastic unitarity condition and the N/D method, with dynamical input from χEFT and the timelike pion form factor measured in e^+e^- annihilation experiments [9,10]. The method effectively includes the ρ meson resonance in the $\pi\pi$ channel, which plays an essential role in electromagnetic structure. It permits calculation of the isovector peripheral densities down to distances $b \gtrsim 1\,\mathrm{fm}$ with controled accuracy. In this article we review the results of the method for the hyperon densities and their impact on the understanding of peripheral hyperon structure. Further applications of the method are described in Refs. [11,12].

2 Formalism

The matrix element of the electromagnetic current between spin-1/2 baryon states with 4-momenta p and p' is described by two form factors, $F_1^B(t)$ and $F_2^B(t)$ (Dirac and Pauli form factors). They are functions of the invariant momentum transfer $t = \Delta^2 = (p' - p)^2$ and can be measured and interpreted without specifying a particular form of relativistic dynamics or reference frame. In the light-front form of relativistic dynamics one follows the evolution of strong interactions in light-front time $x^+ \equiv x^0 + x^3$ [13–15]. In this context

it is natural to consider the form factors in a frame where the 4-momentum transfer has only transverse components $\boldsymbol{\Delta}_T = (\Delta^x, \Delta^y), |\boldsymbol{\Delta}_T|^2 = -t$, and to represent them as Fourier transforms of two-dimensional spatial densities

$$F_i^B(t = -|\boldsymbol{\Delta}_T|^2) \;=\; \int d^2b\; e^{i\boldsymbol{\Delta}_T\cdot\boldsymbol{b}}\; \rho_i^B(b) \qquad (i = 1, 2), \tag{1}$$

where $\boldsymbol{b} \equiv (b^x, b^y)$ is a transverse coordinate variable and $b \equiv |\boldsymbol{b}|$. The functions $\rho_1^B(b)$ and $\rho_2^B(b)$ describe the transverse spatial distribution of charge and magnetization in the baryon at fixed $x^+ = 0$ and are invariant under boosts in the z-direction. Their interpretation as spatial densities and other properties have been discussed extensively in the literature [5,6,8,16]. Alternative to the magnetization density $\rho_2^B(b)$ one also considers the function

$$\widetilde{\rho}_2^B(b) \equiv \frac{\partial}{\partial b}\left[\frac{\rho_2^B(b)}{2m_B}\right], \tag{2}$$

which has a simple partonic interpretation. Together, $\rho_1^B(b)$ and $\widetilde{\rho}_2^B(b)$ contain the full information about the current matrix element and provide a concise spatial representation of the baryons' electromagentic structure.

The baryon form factors are analytic functions of t and have a dispersive representation of the form

$$F_i^B(t) \;=\; \int_{t_{\rm thr}}^{\infty} \frac{dt'}{t' - t - i0}\, \frac{\mathrm{Im}\, F_i^B(t')}{\pi} \qquad (i = 1, 2), \tag{3}$$

in which they are expressed as integrals over the imaginary parts (spectral functions) on the cut at $t > t_{\rm thr}$. The spectral functions arise from processes in which the current produces a hadronic state that couples to the baryon-antibaryon system, current $\to$ hadronic state $\to B\bar{B}$. Using this representation in Eq. (1), one obtains a dispersive representation of the densities [17,18]

$$\rho_1^B(b) = \int_{t_{\rm thr}}^{\infty} dt\; \frac{K_0(\sqrt{t}b)}{2\pi}\, \frac{\mathrm{Im}F_1^B(t)}{\pi}, \tag{4}$$

$$\widetilde{\rho}_2^B(b) = -\int_{t_{\rm thr}}^{\infty} dt\; \frac{\sqrt{t}K_1(\sqrt{t}b)}{4\pi m_B}\, \frac{\mathrm{Im}F_2^B(t)}{\pi}. \tag{5}$$

Here K_n $(n = 0, 1)$ are the modified Bessel functions, which decay exponentially at large arguments, $K_n(\sqrt{t}b) \sim (\sqrt{t}b)^{-1/2}\, e^{-\sqrt{t}b}$ for $\sqrt{t}b \gg 1$. The integrals for the densities therefore converge exponentially at large t. The distance b determines at what values of t the spectral function is effectively sampled in the integral ("exponential filter"). In particular, the densities at large distances are governed by the lowest-mass hadronic states in the spectral function. In the isovector densities this is the two-pion state (threshold $t_{\rm thr} = 4\, M_\pi^2$), which includes the ρ resonance at $t \sim 30\, M_\pi^2$; in the isoscalar densities these are effectively the ω and ϕ resonances in the 3π and $K\bar{K}$ channels. The densities thus enable a parametric definition of "peripheral" baryon structure and relate it to the spectral decomposition of the form factors.

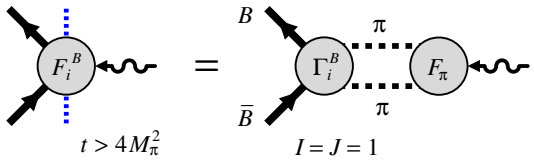

Fig. 1 Unitarity relation for the isovector spectral function on the two-pion cut.

The isovector spectral functions on the two-pion cut can be computed in a new approach based on elastic unitarity, the N/D method, and dynamical input from χEFT and timelike pion form factor measurements [9]. The elastic unitarity condition in the two-pion channel allows one to express the spectral functions as [19–21]

$$\mathrm{Im}F_i^B(t) = \frac{k_{\rm cm}^3}{\sqrt{t}}\, \Gamma_i^B(t)\, F_\pi^*(t) \qquad (i = 1, 2), \tag{6}$$

where $k_{\rm cm} = \sqrt{t/4 - M_\pi^2}$ is the center-of-mass momentum of the $\pi\pi$ system in the t-channel, $\Gamma_i^B(t)$ is the $I = J = 1$ $\pi\pi \to B\bar{B}$ partial wave amplitude, and $F_\pi(t)$ is the pion timelike form factor (see Fig. 1). The complex amplitudes $\Gamma_i^B(t)$ and $F_\pi(t)$ have the same phase on the two-pion cut; the phase arises from $\pi\pi$ rescattering in the t-channel, which affects both amplitudes in the same way (Watson theorem) [22]. The unitarity condition Eq. (6) can thus be written in manifestly real form as

$$\mathrm{Im}F_i^B(t) = \frac{k_{\rm cm}^3}{\sqrt{t}}\, \frac{\Gamma_i^B(t)}{F_\pi(t)}\, |F_\pi(t)|^2 \qquad (i = 1, 2). \tag{7}$$

The ratio $\Gamma_i^B(t)/F_\pi(t)$ is real and free of $\pi\pi$ rescattering effects. This function can be computed in χEFT with relativistic baryons with controled accuracy. The factor $|F_\pi(t)|^2$ contains the $\pi\pi$ rescattering effects and the ρ resonance, and is taken as the empirical form factor measured in e^+e^- annihilation experiments. The approach allows us to construct the two-pion spectral functions of baryons in the region $4M_\pi^2 < t \lesssim 1\,\mathrm{GeV}^2$, which includes the ρ meson resonance. Further aspects of the method are discussed in Refs. [9,12,11].

The isovector spectral functions of the $SU(3)$ octet baryons have been calculated with the above method, using relativistic χEFT with spin-1/2 octet and spin-3/2 decuplet baryons in LO accuracy [9]. The chiral processes contributing to partial-wave amplitudes $\Gamma_i^B(t)$ at this accuracy are shown in Fig. 2. [Calculations in the $SU(2)$ sector have meanwhile been extended to NLO and partial N2LO accuracy and show good convergence in higher orders [12].] The isoscalar spectral functions have been modeled by vector meson exchange (ω, ϕ), with couplings constrained by $SU(3)$ symmetry and dispersive fits to the nucleon form factor data [9].[1] With these spectral functions we

[1] The contribution of $K\bar{K}$ states to the hyperon isovector and isoscalar spectral functions in χEFT was computed in Ref. [23] without rescattering effects. The contributions of these states to the peripheral densities considered here turns out to be negligible.

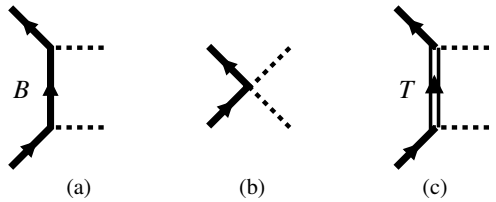

Fig. 2 LO χEFT diagrams contributing to the $\pi\pi \to N\bar{N}$ partial-wave amplitudes Γ_i^B in the $I = J = 1$ channel. (a) Born term with intermediate octet baryon B. (b) Weinberg-Tomozawa contact term. (c) Born term with intermediate decuplet baryon T.

have evaluated the peripheral transverse densities of the hyperons through the dispersive representation Eqs. (4) and (5).

3 Results and discussion

The results for the hyperon charge densities $\rho_1^B(b)$ and magnetization densities $\widetilde{\rho}_2^B(b)$ are summarized in Figs. 3 and 4. The baryons in the octet representation of $SU(3)$ form four isospin multiplets

$$\left.\begin{array}{ccc} \text{multiplet} & \text{baryons} & \text{isospin} \\ N & p, n & I = \frac{1}{2} \\ \Lambda & \Lambda & I = 0 \\ \Sigma & \Sigma^+, \Sigma^-, \Sigma^0 & I = 1 \\ \Xi & \Xi^0, \Xi^- & I = \frac{1}{2}. \end{array}\right\} \tag{8}$$

Within each multiplet we write the densities as the sum/difference of an isoscalar and isovector component,

$$\left.\begin{array}{rl} \{\rho^p, \rho^n\} &= \rho^{N,S} \pm \rho^{N,V}, \\ \rho^{\Lambda} &= \rho^{\Lambda,S}, \\ \{\rho^{\Sigma^+}, \rho^{\Sigma^-}\} &= \rho^{\Sigma,S} \pm \rho^{\Sigma,V}, \\ \rho^{\Sigma^0} &= \rho^{\Sigma,S}, \\ \rho^{\Lambda-\Sigma} &= \rho^{\Lambda-\Sigma,V}, \\ \{\rho^{\Xi^0}, \rho^{\Xi^-}\} &= \rho^{\Xi,S} \pm \rho^{\Xi,V}. \end{array}\right\} \tag{9}$$

The Λ and Σ^0 densities are pure isoscalar, while the Λ-Σ^0 transition form factors are pure isovector. For each hyperon B we show the total densities as well as their isovector and isoscalar components.

The peripheral densities decay exponentially in b, as expected from the analytic properties of Eqs. (4) and (5). The decay rate is determined by the effective t-values in the spectral integral. The isovector densities decay approximately as $\sim \exp(-M_\rho b)$ at $b \sim 1$ fm, and with a smaller effective mass at $b > 2\,\text{fm}$, because at larger b the spectral integral shifts to smaller t-values closer to the two-pion threshold. The isoscalar densities always decay with the

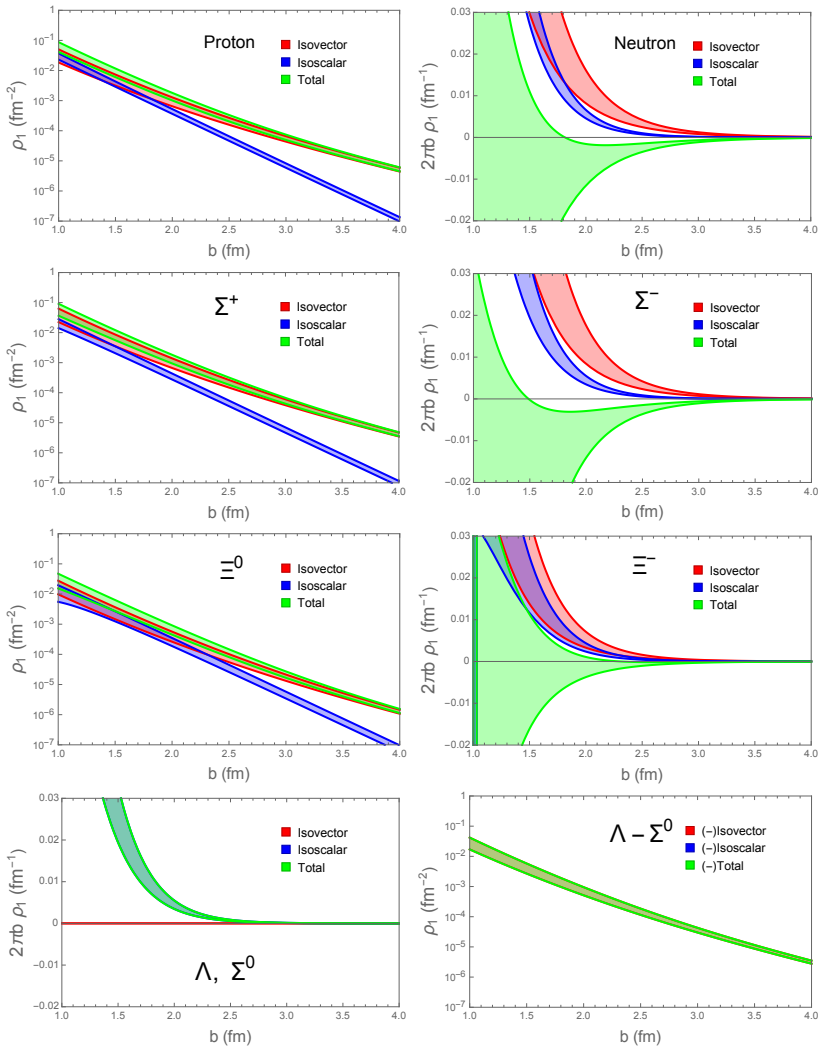

Fig. 3 Peripheral transverse charge densities of the octet baryons [9]. Red: Isovector component calculated with the spectral functions obtained from Eq. (7), χEFT, and the empirical pion form factor. Blue: Isoscalar component estimated from vector meson poles. Green: Total density (sum or difference of isoscalar and isovector components). For the densities with fixed sign we plot $\rho_1(b)$ on a logarithmic scale (the signs are indicated in the legends of the plots); for those with changing sign we plot the radial densities $2\pi b\rho_1(b)$ on a linear scale.

ω mass. As a consequence, the overall densities are dominated by the isovector component at distances $b > 3$ fm. Since this component can be calculated model-independently, we are able to predict the overall densities in this region within our approach [9]. Isoscalar and isovector densities become comparable only at distances $b < 2$ fm. In this region the uncertainties of our isovector cal-

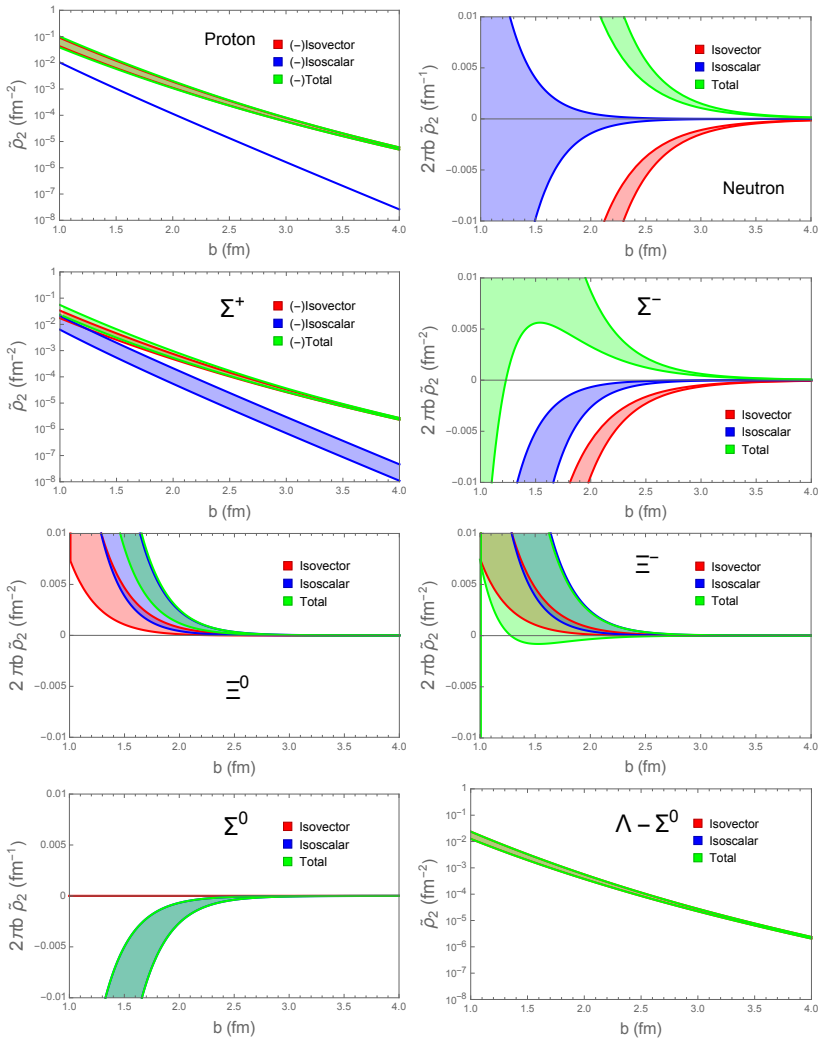

Fig. 4 Peripheral transverse magnetization densities of the octet baryons. For color coding and explanations see Fig. 3.

culation become larger, and the model dependence of the isoscalar component is significant.

The charge densities of the Σ^+ and Σ^- show very similar behavior to those in the proton and neutron. In both cases isovector and isoscalar components are present. In the p and Σ^+ the isovector and isoscalar contribute with the same sign, while in the n and Σ^- they contribute with different sign. This gives rise to a uniform charge density in the p and Σ^+, and to a more complex behavior in the n and Σ^-. A sign change in the neutron charge density, from negative at large b to positive at $b \sim 1$ fm, was observed in the empirical

densities [7,18]. Our results are consistent with this finding, but the present accuracy does not allow us to predict the sign at $b < 2$ fm. A similar sign change might be present in the Σ^- density.

Our calculation shows that the peripheral isovector charge density in the charged Σ multiplet is very close to that in the nucleon multiplet. This comes about due to two circumstances: (a) the isospin factors in the $\pi BB'$ couplings entering in the Born graphs of Fig. 2; (b) the relative contribution of intermediate octet and decuplet states; see Ref. [9] for a detailed discussion. Similar behavior is observed in the Σ magnetization densities [9]. Overall this shows that the "pion cloud" in the charged Σ hyperons is of comparable size as in the nucleon.

In the Ξ hyperons the peripheral isovector charge density is substantially smaller than in the nucleon and charged Σ states. The reason is that the intermediate octet contribution to the Ξ Born graphs is small and comparable to the decuplet one. The isoscalar density in the Ξ is of normal size. This has interesting implications for the charge density in the Ξ^-, which is the difference of the isoscalar and isovector components. It suggests a sign change from a negative charge density at large b to a positive one at intermediate b, similar to the neutron and Σ^-, but with the transition occuring at larger b than in the neutron or Σ^- (we cannot confirm this behavior with the present uncertainties). Similar behavior is observed in the Ξ magnetization densities [9]. Overall this means that the "pion cloud" in the Ξ is substantially smaller than in the nucleon and charged Σ.

In the Λ and Σ^0 densities the isovector component is absent in both the charge and the magnetization densities, see Eq. (9). In the χEFT calculation this comes about through the cancellation of the π^+ and π^- contributions in the Born graphs with intermediate octet and decuplet states. The Λ and Σ^0 densities are thus pure isoscalar, and dominated by ω and ϕ exchange in the whole range considered. This has as consequence that the peripheral densities are overall an order of magnitude smaller than for the other hyperons at $b > 2$ fm. The Λ and Σ^0 are therefore more compact objects than the other hyperons as far as electromagnetic structure is concerned. (We note that isospin symmetry breaking would resulting in a small long-range component of the Λ and Σ^0 densities and qualitatively change their asymptotic behavior [9].) The charge densities have the same sign for both Λ and Σ^0, while the magnetization densities have opposite sign.

The Λ-Σ^0 transition densities are of particular interest because of their pure isovector nature. They receive sizable peripheral contributions from the chiral processes with octet and decuplet intermediate states. These densities can be computed model-independently down to distances $b \sim 1$ fm and represent genuine predictions of our approach. It would therefore be interesting to compare our results to those of other approaches that describe baryon structure in the central region $b < 1$ fm, such as quark models. The electromagnetic form factors of the hyperons are being studied also in Lattice QCD [24–26]. If such calculations could determine the transverse densities in a region where both our and their approach are reliable, the results could be

matched directly. Note also that the Λ-Σ^0 transition form factor is accessible experimentally through the Dalitz decay $\Sigma^0 \to \Lambda e^+ e^-$ at timelike momentum transfers $4m_e^2 < t < (m_{\Sigma^0} - m_\Lambda)^2 = 0.006\,\mathrm{GeV}^2$ [27]. Such measurements may be able to determine a combination of the slopes of the magnetic and electric transition form factors at $t = 0$ (magnetic and electric radii), which could be compared with dispersive calculations using the spectral functions computed in our approach [9] and Ref. [10].

Using similar methods one can determine also the quark flavor decomposition of the transverse densities in the hyperon states [9]. This analysis requires additional assumptions about the quark composition of the isoscalar ω and ϕ exchanges (ideal mixing) and is more model-dependent. The ratios of the flavor densities show the transition from the "pion cloud" at $b > 3$ fm to a "mean-field picture" of valence quarks at $b \sim 1$ fm, as observed earlier in the nucleon densities [18]. These results can be used to further quantify the "pion cloud" in hyperons; see Ref. [9] for details.

4 Summary

Transverse densities enable a model-independent definition of peripheral baryon structure and its dynamical content. Using a new method combining χEFT and dispersion analysis, we have computed the peripheral isovector charge and magnetization densities in hyperons resulting from the two-pion cut of the form factors. The method includes $\pi\pi$ rescattering and the ρ resonance and allows us to construct the isovector densities with controled accuracy down to $b \sim 1$ fm.

Our results show that the "pion cloud" in the charged Σ hyperons is generally as large as that in the nucleon, while that in the Ξ hyperons is substantially smaller. The pattern is caused by the isospin factors in the $\pi BB'$ couplings and the relative contribution of intermediate octet and decuplet states in the Born graphs. Detailed tests of the dynamics can be performed by studying different b-regions and comparing charge and magnetization densities. The Λ–Σ^0 transition density is pure isovector and represents a clean expression of peripheral two-pion dynamics.

The results reported here were obtained using LO χEFT. Calculations in the $SU(2)$ sector at NLO and partial N2LO accuracy and show good convergence in higher orders [12]. This will allow us to substantially reduce the theoretical uncertainty in the predicted transverse densities. The method can also be extended to other baryon form factors, such as the scalar form factor [11].

Acknowledgements

This material is based upon work supported by the U.S. Department of Energy, Office of Science, Office of Nuclear Physics under contract DE-AC05-06OR23177, and by the Deutsche Forschungsgemeinschaft DFG. It was also

funded by MINECO (Spain) and the ERDF (European Commission) grants No. FIS2014-51948-C2-2-P and SEV-2014-0398, and by the Generalitat Valenciana under Contract PROMETEOII/2014/0068.

References

1. J. Lach and P. Zenczykowski, Int. J. Mod. Phys. A **10**, 3817 (1995). doi:10.1142/S0217751X95001807
2. N. Cabibbo, E. C. Swallow and R. Winston, Ann. Rev. Nucl. Part. Sci. **53**, 39 (2003) doi:10.1146/annurev.nucl.53.013103.155258 [hep-ph/0307298].
3. C. B. Dover and A. Gal, Prog. Part. Nucl. Phys. **12**, 171 (1985) doi:10.1016/0146-6410(84)90004-8
4. D. E. Soper, Phys. Rev. D **15**, 1141 (1977). doi:10.1103/PhysRevD.15.1141
5. M. Burkardt, Phys. Rev. D **62**, 071503 (2000) Erratum: [Phys. Rev. D **66**, 119903 (2002)] doi:10.1103/PhysRevD.62.071503, 10.1103/PhysRevD.66.119903 [hep-ph/0005108].
6. M. Burkardt, Int. J. Mod. Phys. A **18**, 173 (2003) doi:10.1142/S0217751X03012370 [hep-ph/0207047].
7. G. A. Miller, Phys. Rev. Lett. **99**, 112001 (2007) doi:10.1103/PhysRevLett.99.112001 [arXiv:0705.2409 [nucl-th]].
8. G. A. Miller, Ann. Rev. Nucl. Part. Sci. **60**, 1 (2010) doi:10.1146/annurev.nucl.012809.104508 [arXiv:1002.0355 [nucl-th]].
9. J. M. Alarcón, A. N. Hiller Blin, M. J. Vicente Vacas and C. Weiss, Nucl. Phys. A **964** (2017) 18 doi:10.1016/j.nuclphysa.2017.05.002 [arXiv:1703.04534 [hep-ph]].
10. C. Granados, S. Leupold and E. Perotti, arXiv:1701.09130 [hep-ph].
11. J. M. Alarcón and C. Weiss, Phys. Rev. C **96** (2017) no.5, 055206 doi:10.1103/PhysRevC.96.055206 [arXiv:1707.07682 [hep-ph]].
12. J. M. Alarcón and C. Weiss, arXiv:1710.06430 [hep-ph].
13. P. A. M. Dirac, Rev. Mod. Phys. **21**, 392 (1949). doi:10.1103/RevModPhys.21.392
14. H. Leutwyler and J. Stern, Annals Phys. **112**, 94 (1978). doi:10.1016/0003-4916(78)90082-9
15. S. J. Brodsky, H. C. Pauli and S. S. Pinsky, Phys. Rept. **301**, 299 (1998) doi:10.1016/S0370-1573(97)00089-6 [hep-ph/9705477].
16. C. Granados and C. Weiss, JHEP **1401**, 092 (2014) doi:10.1007/JHEP01(2014)092 [arXiv:1308.1634 [hep-ph]].
17. M. Strikman and C. Weiss, Phys. Rev. C **82**, 042201 (2010) doi:10.1103/PhysRevC.82.042201 [arXiv:1004.3535 [hep-ph]].
18. G. A. Miller, M. Strikman and C. Weiss, Phys. Rev. C **84**, 045205 (2011) doi:10.1103/PhysRevC.84.045205 [arXiv:1105.6364 [hep-ph]].
19. W. R. Frazer and J. R. Fulco, Phys. Rev. **117**, 1603 (1960). doi:10.1103/PhysRev.117.1603
20. Phys. Rev. **117**, 1609 (1960). doi:10.1103/PhysRev.117.1609
21. G. Hohler and E. Pietarinen, Nucl. Phys. B **95**, 210 (1975). doi:10.1016/0550-3213(75)90042-5
22. K. M. Watson, Phys. Rev. **95**, 228 (1954). doi:10.1103/PhysRev.95.228
23. A. N. Hiller Blin, Phys. Rev. D **96**, no. 9, 093008 (2017) doi:10.1103/PhysRevD.96.093008 [arXiv:1707.02255 [hep-ph]].
24. H. W. Lin and K. Orginos, Phys. Rev. D **79**, 074507 (2009) doi:10.1103/PhysRevD.79.074507 [arXiv:0812.4456 [hep-lat]].
25. P. E. Shanahan *et al.* [CSSM and QCDSF/UKQCD Collaborations], Phys. Rev. D **89**, 074511 (2014) doi:10.1103/PhysRevD.89.074511 [arXiv:1401.5862 [hep-lat]].
26. P. E. Shanahan *et al.*, Phys. Rev. D **90**, 034502 (2014) doi:10.1103/PhysRevD.90.034502 [arXiv:1403.1965 [hep-lat]].
27. M. F. M. Lutz *et al.* [PANDA Collaboration], arXiv:0903.3905 [hep-ex].